Evaporation of suspended nanofluid (SiO_2/water) droplets: experimental results and modelling

E.M. Starinskaya[1†], N.B. Miskiv[1†], A.D. Nazarov[1†], V.V. Terekhov[1†], V.I. Terekhov[1†], O.D. Rybdylova[2†] and S.S. Sazhin[2*†]

[1*]Kutateladze Institute of Thermophysics, Novosibirsk, 630090, Russian Federation.
[2]Advanced Engineering Centre, School of Architecture, Technology and Engineering, University of Brighton, Brighton, BN2 4GJ, UK.

*Corresponding author(s). E-mail(s): S.Sazhin@brighton.ac.uk;
Contributing authors: prefous-lm@yandex.ru; nikerx@gmail.com; nazarov@itp.nsc.ru; vt@itp.nsc.ru; terekhov@itp.nsc.ru; O.Rybdylova@brighton.ac.uk;
†These authors contributed equally to this work.

Abstract

The results of experimental studies and modelling of the evaporation of suspended water droplets containing silicon dioxide SiO_2 nanoparticles at mass fractions 0.02 and 0.07 are presented. The experimental results are analysed using the previously developed model for multicomponent droplet heating and evaporation. In this model droplets are assumed to be spherical and the analytical solutions to the heat transfer and species diffusion equations are incorporated into the numerical code. They are used at each timestep of the calculations. Silicon dioxide nanoparticles are considered to be a non-evaporating component. It is demonstrated that both experimental and predicted values of droplet diameters to the power 1.5 decrease almost linearly with time, except at the beginning and the final stages of the evaporation process, and are only weakly affected by the presence of nanoparticles. At the final point in this process, the effect of nanoparticles becomes dominant when their mass fraction at

the droplet surface reaches about 40% and a cenosphere-like structure is formed. Both predicted and observed droplet surface temperatures rapidly decrease during the initial stage of droplet evaporation. After about $\boldsymbol{t = 100}$ s the predicted surface temperature remains almost constant while its experimentally observed values increase with time. This might be related to a decrease in the temperature of ambient air in the vicinity of droplets, not taken into account in the model. Both observed and predicted values of the mass fraction of silicon dioxide at the droplet surfaces are shown to increase with time until they reach about 0.4.

1 Introduction

Experimental studies and modelling of nanofluids have become a new and rapidly growing direction of research in the last two decades [1]-[6]. These nanofluids are now considered to be promising coolants in heat exchangers, heat pipes, solar collectors and many other energy devices. The most powerful effects of nanoparticles can be exerted in two-phase (gas-liquid) systems and especially in the presence of phase changes – boiling and evaporation. In this case, nanoparticles at the interfacial boundaries can have an important impact on the surface forces, as a result of which the magnitude of the critical heat fluxes during the boiling of the nanofluids can change greatly compared to those of pure liquids. This can affect the rate of droplet evaporation [4, 7–9].

Note that so far research into nanofluids has been focused mainly on convective heat exchange in the single-phase mode rather than on their phase transformation. Evaporation of both suspended and sessile nanofluid droplets, for which the processes at the interfacial boundary can play a significant role, were investigated by Zhong et al. [10] and Sefiane and Bennacer [11]. Evaporation of these droplets can be affected by several parameters, including the composition of the base fluid, size, shape, material, and concentration of nanoparticles, and the surface tension, speed and temperature of the surrounding flow [12]. Despite the existence of a number of available theoretical and experimental publications on the evaporation of nanofluids, this field of science is still being developed.

Chen et al. [13, 14] were among the first to present the results of measurements of the rate of evaporation and surface tension of droplets of nanofluids suspended from a capillary. Laponite (mass fraction 0.5%), Ag (silver) and Fe_2O_3 (mass fractions 0.05%) nanoparticles were added to the base fluid (water). To stabilize the nanofluid with silver (diameters in the range 10-30 nm) and iron oxide (diameters in the range 30-40 nm) nanoparticles, polyvidone (PVP) was used as a surfactant (mass fraction 1%). The presence of a surfactant stimulated an approximate doubling of the droplet evaporation rate. The weak effect of the addition of nanoparticles on the droplet surface tension, and the rate of their initial evaporation was demonstrated. When a certain critical size was reached, the rate of droplet evaporation decreased, and

this effect was most visible for solutions with silver nanoparticles. For laponite, there was no change in the droplet evaporation rate; the nanofluid with Fe_2O_3 nanoparticles occupied an intermediate position between them.

The impact of nanoparticles on the evaporation rate of silicone oil and deionized water was investigated experimentally by Zhang et al. [15]. Nanoparticles of silicon dioxide (SiO_2), calcium titanate ($CaTiO_3$) and two modifications of titanium dioxide (TiO_2) (anatase and rutile) were used. It was shown that the presence of nanoparticles could suppress or intensify the evaporation of a water-based nanofluid with TiO_2 anatase nanoparticles, depending on their concentration. The process of flotation of nanoparticles on the surface of the liquid was considered in more detail by Bochkarev and Polyakova [16].

Kumar and Sathian [17] used non-equilibrium molecular dynamics methods to investigate the evaporation of liquid argon droplets with platinum nanoparticles. The authors analysed in detail the contribution of each input parameter and showed that an increase in the interaction force at the nanoparticle - base liquid boundary leads to a decrease in the evaporation intensity. A phenomenological model based on the theory of convective nanofluid drying was developed by Wei et al. [18]. Handscomb et al. [19] developed a drying model of a droplet of colloidal liquid when a porous structure was formed during the final stage of droplet evaporation.

The evaporation of nanofluids with nanoparticles of diamond, oxides of silicon, aluminum and zirconium was investigated experimentally by Minakov et al. [20]. Terekhov and Shishkin [21] showed experimentally that the presence of carbon nanotubes in low concentration does not affect the droplet evaporation rate.

As follows from the experimental results presented by Moghiman and Aslani [22], the addition of small amounts of nanoparticles to a base liquid can lead to an intensification of the evaporation process or its suppression, or have no influence on it whatsoever. As follows from the results presented in [23], the rate of droplet evaporation depends on the specific material of the nanoparticles, the presence of stabilizing additives and a number of other factors.

There were several studies of evaporation and combustion of fuel droplets with nanoparticles from high-energy materials including aluminium with surface protection [23–25], cerium [26] and its oxide [27], and graphite [28]. The contribution of nanoparticles to the transfer of thermal radiation in nanofluids was investigated by Gan and Qiao [29], Said et al. [30], and Jing and Song [31].

Numerical modelling of nanofluid droplets has been discussed in a number of papers including [25]. Wei et al. [18] and Fisenko and Khodyko [32] drew attention to the fact that accumulation of nanoparticles in the vicinity of the droplet surface leads to a reduction in the effective area of droplet evaporation which leads to a reduction in the rate of evaporation. Note that most attention has been focused on sessile droplets [6, 33, 34], the analysis of which is beyond the scope of this paper.

As follows from the brief review of previous research into the heating and evaporation of nanofluid droplets presented above, this problem is far from well understood. Even at a qualitative level, it is difficult to predict the nature of the change in the rate of evaporation of droplets containing nanoparticles of various materials, sizes, and shapes. The aim of this paper is to make a further contribution to this study and clarify some features of nanofluid droplet evaporation which have not been considered so far.

The paper focuses on the experimental study and modelling of the evaporation of suspended water droplets, containing silicon dioxide SiO_2 nanoparticles with mass fractions 0.02 and 0.07, in an ambient temperature of 28.4°C (room temperature), airflow velocity $U = 0.2 \pm 0.02$ m/s and relative humidity 4.3%.

The choice of mass fractions of nanoparticles was motivated by our intention to investigate the effect of a high concentration of nanoparticles on the nanofluid droplet evaporation process, including the formation of the cenosphere-like structure during their evaporation. This study is complementary to the previous investigation where the effect of low mass fraction (0.1%) of these particles was investigated [35]. The initial mass fractions of nanoparticles 0.02 and 0.07 were chosen based on the observation that for these values their agglomeration was not observed until the final stage of the drying process when the cenosphere-like structure was formed. The relative humidity used in our experiments was the lowest that we could effectively control. The chosen air velocity was the lowest for which the effect of ambient conditions outside the chamber where the experiments were performed on the droplet evaporation process could be ignored.

This study was primarily motivated by the fact that silicon oxide nanopowders are widely used in various fields of industry and science. They are actively used as additives in paint products, anti-corrosion, antifriction and hydrophobic coatings, and rubber products. SiO_2 nanoparticles are used as additives for concretes, dry building mixtures, heat-resistant and heat-insulating materials [36].

2 Experimental setup and procedure

A scheme of the experimental setup is presented in Figure 1. A liquid droplet was fixed on a crosshair of threads with diameters 105 μm, and placed above a nozzle. The thread material (horsehair) had a fairly low thermal conductivity (about 0.15 W/(m K)) and did not absorb water [37]. Heat supplied through these threads was assumed to be small [38]. This type of support allowed us to preserve the spherical shape of the droplet during most of the evaporation process. Also, it prevented droplet movement along the thread and reduced its vibration in the airflow [39].

The gas flow came from a compressed air cylinder into the heating section through a cylindrical channel with a diameter of 150 mm. Then it passed through a narrowing channel with a diameter of 60 mm. The inlet flow rate was controlled by a reducer. To reduce disturbances in the flow, the gas passed

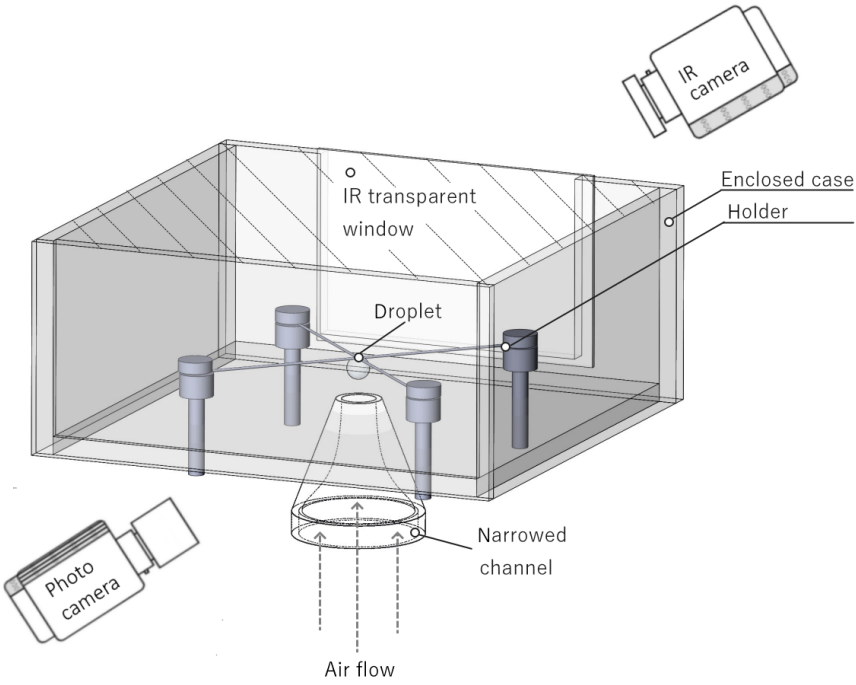

Fig. 1 The scheme of the setup used in the experiments.

through a system of two honeycombs with grid steps 0.5 mm and 0.2 mm. These honeycombs were located at a distance of 380 mm from each other. A profiled converging channel (confuser) was installed at the exit from the working area. This confuser had an outlet diameter of 12 mm and the degree of flow compression was 17. It ensured the formation of a homogeneous flow.

Airflow speed was measured with a KIMO instruments VT110 anemometer at the outlet from the confuser. The anemometer and a rotameter allowed us to perform measurements of velocity in the range $0.1 - 3$ m/s with uncertainty $\pm 3\%$. The values of relative humidity ϕ at the location of the droplet were measured with a hygrometer probe (AZ Instrument model 872) with measurement uncertainty $\pm 4\%$. A closed box shown in Figure 1 was used in the experiments to ensure that ϕ remained constant (cf. [40]).

The time evolution of droplet radii was measured with a Baumer vcxg-04m high-speed video camera. The obtained data were processed using the ImageJ program. Approximating the droplet shapes by that of a spheroid their diameters (d) were estimated as:

$$d = \left(a^2 b\right)^{1/3},$$

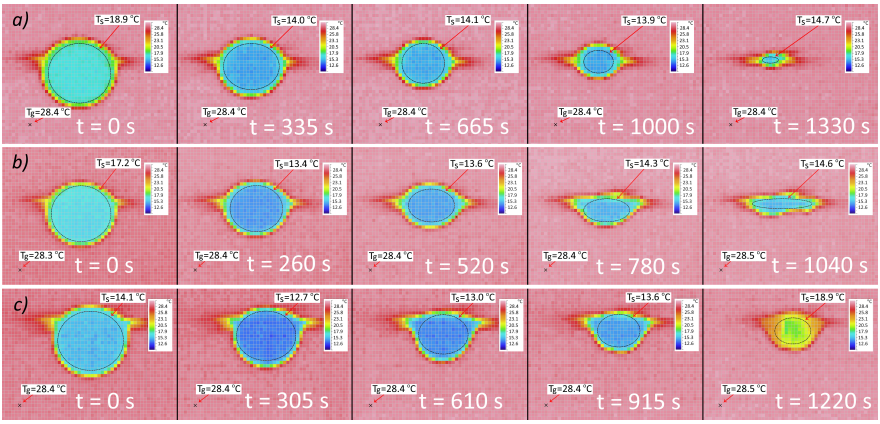

Fig. 2 Typical droplet images obtained using the thermal imaging camera for pure water (a) and nanofluids with mass fractions of nanoparticles 0.02 (b) and 0.07 (c) obtained at various time instants. Gas temperatures are shown for all cases.

where a and b are the axes of the spheroid. The measurement uncertainty did not exceed ± 0.07 mm.

The sources of errors of measurements of d include systematic errors (e.g. those related to non-sphericity of droplets), and random errors. These were estimated as 0.05 mm and 0.02 mm, respectively, in the range of droplet diameters under consideration, and were considered to be additive, leading to the above-mentioned measurement uncertainty of ± 0.07 mm. The dependence of these errors on droplet sizes was weak and not considered in our analysis. This led to errors of $(d/d_0)^{1.5}$ equal to $1.5(0.07/2) = 1.5 \times 0.035 \approx 0.05$ at the beginning of the evaporation process. These errors increased to about 0.1 at the end of this process.

The droplet diameters were measured simultaneously with the measurements of temperatures in the vicinity of droplet surfaces. These temperatures were measured with an NEC TH7102IR thermal imaging camera at wavelengths $\lambda = 8 - 14$ μm using a TH 71-377 macro lens. These temperature measurements refer to droplet surfaces with a thickness of not more than 9 μm. The value of this thickness was determined by the depth of the IR penetration into the droplet at various wavelengths [41].

The thermal imaging camera was installed with a focal length of 6 cm [41–43]. Individual temperature measurements were averaged over the area near the central part of the thermal image of the droplet. The data were processed by ThermoTracer software. The systematic and random errors of these measurements were estimated to be 0.2 K and 0.45 K, respectively, leading to a total error of 0.65 K. See [41]-[43] for a more detailed analysis of methods of droplet temperature measurement using thermal imaging.

Typical images of droplets of pure water and nanofluids obtained using this camera are shown in Figure 2. As follows from this figure, in all cases the droplet surface temperature first drops and then gradually increases during the evaporation process. The formation of the cenosphere-like structure can

be clearly seen for the nanofluid droplet with a mass fraction of nanoparticles equal to 0.07.

The average mass fractions of nanoparticles were estimated as

$$Y_l = Y_{l0} \left(d_0/d\right)^3,$$

where Y_{l0} is the initial mass fraction (0.02 or 0.07) of nanoparticles, d_0 is the initial droplet diameter. The errors of measurements of Y_{l0} did not exceed 0.5% for $Y_{l0} = 0.02$ and 0.1% for $Y_{l0} = 0.07$. The error of measurement of $(d_0/d)^3$ was $3(0.07/2) = 3 \times 0.035 \approx 0.1$ at the beginning of the evaporation process and increased to about 0.2 at the final stages of this process. This means that the latter errors control the overall errors of measurement of Y_{l0} and are equal to approximately 10% (beginning of the evaporation process) or 20% (end of the evaporation process) for both Y_{l0}.

Nanofluids used in the experiments were prepared based on commercially available spherical nanoparticles of silicon dioxide (SiO_2) with median diameters 12 nm supplied by the Evonik company. This size was the result of a compromise between availability and the requirement to minimise particle sizes. Distilled water was used as the base liquid. To prepare nanofluids with certain mass fractions of components the latter were weighed on HR-250AZG electronic scales with measurement error ± 0.1 mg. Then the nanoparticles and base liquid were mixed manually. An ultrasonic treatment was used to obtain a stable homogeneous mixture with a minimum degree of particle agglomeration [23]. Note that all nanofluids were prepared without the addition of surfactants.

3 Models and approximations

3.1 Description of models and approximations

The experimental results obtained using the setup and procedures described in Section 2 were analysed using the model of droplet drying developed by the authors of [44] and the model describing the effect of support presented in [45]. In the model described in [44], nanoparticles inside water in droplets are considered to be a non-evaporating liquid.

The spherically symmetric processes inside the droplet were described based upon the transient heat transfer and species diffusion equations [46]:

$$\frac{\partial T}{\partial t} = \kappa_{\text{eff}} \left(\frac{\partial^2 T}{\partial R^2} + \frac{2}{R} \frac{\partial T}{\partial R} \right) + P, \tag{1}$$

$$\frac{\partial Y_{li}}{\partial t} = D_{\text{eff}} \left(\frac{\partial^2 Y_{li}}{\partial R^2} + \frac{2}{R} \frac{\partial Y_{li}}{\partial R} \right), \tag{2}$$

where $T \equiv T(R,t)$ and $Y_{li} \equiv Y_{li}(R,t)$ are the temperature and mass fractions of water ($_{i=0}$) and nanoparticles ($_{i=1}$) inside the droplets, R and t are the distance from the droplet centre and time, respectively, and κ_{eff} and D_{eff} are

effective thermal and nanoparticle diffusivities, respectively. These diffusivities consider the effects of recirculation inside droplets due to their motion relative to the gas, using the Effective Thermal Conductivity (ETC) and Effective Diffusivity (ED) models [46]. $P \equiv P(R,t)$ accounts for the effects of external heating inside droplets (e.g. thermal radiation).

Equations (1) and (2) were solved analytically assuming that $T(R,t)$ and $Y_{li}(R,t)$ are twice continuously differentiable functions at $0 \le R \le R_d$ (R_d is the droplet radius), using the standard initial conditions and the following conditions at the droplet surface:

$$h(T_g - T_{\text{eff}}) = k_{\text{eff}} \frac{\partial T}{\partial R}(R = R_d), \tag{3}$$

$$\frac{\partial Y_{li}}{\partial R}(R = R_d) = \frac{\dot{m}_d}{4\pi R_d^2 D_{\text{eff}} \rho_l} \left(Y_{li} - \varepsilon_i\right). \tag{4}$$

where

$$T_{\text{eff}} = T_g + \frac{\rho_{l0} L \dot{R}_d}{h}, \qquad \dot{R}_d = \frac{\dot{m}_d}{4\pi R_d^2 \rho_{l0}}, \tag{5}$$

$$\varepsilon_0 = \frac{Y_{v0s}}{Y_{v0s} + Y_{v1s}} = 1, \;\; \varepsilon_1 = \frac{Y_{v1s}}{Y_{v0s} + Y_{v1s}} = 0, \;\; (Y_{v0s} = 1, \;\; Y_{v1s} = 0), \tag{6}$$

h and $\dot{m}_d$ are the convection heat transfer coefficient and the rate of droplet evaporation, respectively, k_{eff} and D_{eff} are the effective thermal conductivity and effective diffusivity, respectively, and ρ_{l0} and L are water density and specific heat of water evaporation, respectively. The value of $\dot{m}_d$ predicted by the Abramzon and Sirignano model [47] was used (see [46] for the details).

The explicit expressions for T and Y_{li}, predicted by the analytical solutions, are given in [46]. They were implemented into the numerical code and used at each timestep for calculations of droplet heating and evaporation [44, 46]. This allowed us to take into account the dependence of all input parameters on time and temperature. The advantages of this approach compared with the one based on a purely numerical solution to Equations (1) and (2) are described in [46].

The effect of thermal swelling or contraction was modelled as in [46]. In this approach, the droplet sizes were calculated assuming that the liquid density is the same throughout the droplet; this density was estimated for the average droplet temperature. The contribution of the supporting thread was accounted for using the approach described in [45]. In this approach, the analytical solution to the transient heat transfer equation inside a semi-transparent droplet in the presence of thermal radiation was used to find heat transferred to the droplet via the supporting thread [45, 46]. It was assumed that this heat is instantaneously and homogeneously distributed throughout the whole volume of the droplet. This assumption can be used when the contribution of heat transferred to the droplet through the thread is much smaller than that transferred to it by convection from the the ambient gas. Thus, the analytical solution to the transient heat transfer equation with internal heating (Equation (1)) was used to study droplet heating via the supporting thread.

In this model, the effect of the thread is considered by using the following expression for P in Equation (1) [45]:

$$P(R) = \frac{3k_l(T_{\sup} - T_c)}{4\pi c_l \rho_l R_d^4} S_c. \tag{7}$$

where $T_{\sup}$ and T_c are the temperatures of the thread and at the droplet centre, S_c is the contact area between the droplet and the thread, subscript l (liquid) refers to a mixture of water and nanoparticles.

This approach allowed us to avoid complex 3D calculations of the effects of the support on droplet heating when these effects are small (see [46] for further details).

It was assumed, following [45], that the contact area of the droplet with the thread can be approximated as

$$S_c = 2\pi d_t R_d,$$

where d_t is the thread diameter, R_d the droplet radius. The low thermal conductivity of the supporting thread allows us to assume, following [48], that $T_{\sup} = T_s$, where T_s is the droplet surface temperature. This approach to considering the effect of the supporting thread is more accurate than the one used in [49] where $T_{\sup}$ was identified with the ambient gas temperature.

To estimate the effect of SiO_2 nanoparticles on droplet evaporation, two areas at the surface of the droplet are introduced. These are the areas covered by water (S_w) and particles (S_p). Note that

$$S_w + S_p = 4\pi R_d^2 \tag{8}$$

$$\frac{\rho_p S_p}{\rho_p S_p + \rho_w S_w} = Y_{l1s}, \tag{9}$$

where Y_{l1s} is the mass fraction of nanoparticles at the droplet surface, and ρ_p and ρ_w are the densities of nanoparticles and water, respectively.

Rearranging (8) and (9) we obtain

$$\frac{S_w}{4\pi R_d^2} = 1 - \frac{\rho_w Y_{l1s}}{\rho_p(1 - Y_{l1s}) + \rho_w Y_{l1s}} \equiv \alpha_s. \tag{10}$$

This allows us to present the evaporation rate of a droplet with nanoparticles as:

$$\dot{m}_d = \alpha_s \, \dot{m}_{d(\mathrm{AS})}, \tag{11}$$

where $\dot{m}_{d(\mathrm{AS})}$ is the evaporation rate of water without nanoparticles predicted by the classical Abramzon and Sirignano model [46]. In our analysis we assumed that $\alpha_s = 1$ (nanoparticles are hydrophilic and covered with water at the droplet surface).

As follows from our experiments, droplet diameters stopped reducing when Y_{l1s} reached about 0.4 – 0.6. At this value of Y_{l1s} nanoparticles form a porous

structure through which water can penetrate from the interior of the droplet to its surface. Unfortunately, this process cannot be investigated using the model developed in [44] and it will not be considered in our analysis. Note that in the original version of the model described in [44] it was assumed that solid residue forms a solid ball. In our approach we considered a more general case assuming that the solid substance forms a porous ball after the completion of the drying process.

The maximal observed value of Y_{l1s} (0.6) is less than the maximal random packing density of spherical solids predicted by Radovskii [50]. In the latter paper, the maximal volume fraction of randomly distributed spheres was predicted to be 0.61 (note that the density of nanoparticles is higher than that of water).

Note that the model of droplet drying described in this section was applied here for the first time to the investigation of nanofluid droplet evaporation.

3.2 Transport and thermodynamic properties

The transport and thermodynamic properties of distilled water and their temperature dependencies used in our analysis are described in [49]. The following parameters for SiO_2 nanoparticles were used: density $\rho_p = 2330$ kg/m^3, thermal conductivity $k_p = 1.4$ W/(m K), and specific heat capacity $c_p = 783$ J/(kg K). All these properties apply at room temperature. Their temperature dependence in the conditions of the experiments was negligible.

The density and specific heat capacity of the mixture of water ($i = 0$) and nanoparticles ($i = 1$) was estimated as [44]:

$$\overline{\rho}_l = (1 - \varphi)\rho_{l0} + \varphi\rho_{l1} \tag{12}$$

$$\overline{c}_l = \frac{(1 - \varphi)\rho_{l0}c_{l0} + \varphi\rho_{l1}c_{l1}}{\overline{\rho}_l}, \tag{13}$$

where φ is the volume fraction of nanoparticles

$$\varphi = \frac{Y_{l1}\overline{\rho}_l}{\rho_{l1}}. \tag{14}$$

Following [51], liquid viscosity is estimated as:

$$\overline{\mu}_l = \mu_{l0}(1 + 2.5\varphi), \tag{15}$$

where μ_{l0} is the dynamic viscosity of water ($_{i=0}$).

Formula (15) is not expected to be very accurate but this is not important for our application as the droplet heating and evaporation rates are weak functions of $\overline{\mu}_l$. They do not depend on $\overline{\mu}_l$ for stationary droplets.

It is assumed that dissolved non-evaporating substances can be treated similarly to non-dissolved substances with masses of particles equal to molecular masses. Thus, the liquid diffusion coefficient can be estimated based on

the Wilke-Chang formula [53]:

$$D_l = \frac{7.4 \times 10^{-15} \sqrt{\overline{M}_v} T}{\mu_l V_v^{0.6}}, \tag{16}$$

where $\overline{M}_v$ is the average molar mass defined as

$$\overline{M}_v = \left[\sum_{i=0}^{i=1} (Y_i / M_i) \right]^{-1}, \tag{17}$$

$_{i=0}$ refers to water, while $_{i=1}$ refers to SiO_2 nanoparticles,

$$V_v = \left(\frac{\sigma_v}{1.18} \right)^3, \tag{18}$$

σ_v is the Lennard-Jones length (in Å) [46, 54]:

$$\sigma_v = 1.468 \, \overline{M}_v^{0.297}, \tag{19}$$

$\overline{M}_v$ is the average molar mass (in kg/kmole), inferred from (17).

One of the key parameters of the model is the thermal conductivity of the mixture of water and SiO_2 nanoparticles. Several approximations of this parameter have been suggested. For our application, this approximation should satisfy three key conditions. Firstly, in the absence of SiO_2 nanoparticles it should reduce to the thermal conductivity of water. Secondly, it should be reasonably close to the experimentally observed values of this parameter. Thirdly, the values of the thermal conductivity predicted by this approximation should be reasonably close to the values predicted by well tested approximations for volume fractions of SiO_2 nanoparticles φ up to about 0.4 – 0.6 (when the porous structure is expected to begin to form). Following [55], we use the following expression, which satisfies all three conditions:

$$\overline{k}_l = k_0 \left[1 + 3 \frac{(k_1/k_0) - 1}{(k_1/k_0) + 2} \varphi \right]. \tag{20}$$

As in the previous formulae, subscript $_1$ ($_0$) refers to nanoparticles (water).

In the calculations, it was assumed that the evaporation heat of the nanofluid droplet is based on that of the evaporating component (water). Approximations for air properties were taken from [56]. The water saturation pressure was obtained following the Ambrose-Walton corresponding states method. The vapour diffusion coefficient was calculated using the Wilke-Lee method [57].

Note that in our approach the effect of nanoparticles was taken into account via the modification of thermodynamic and transport properties of nanofluids.

The detailed analysis of the processes at the nanoparticle/base liquid interface is beyond the scope of our investigation.

4 Modelling versus experimental data

As in [49], our focus is on droplet surface temperatures (T_s) and their diameters (d). Since all experiments were performed for droplets with initial temperatures equal to the ambient gas temperatures (T_g), which remained almost constant during the experiments, we will present the results for $T_g - T_s$ rather than for T_s. This approach will allow us to show more clearly the conditions in which droplet evaporation takes place. Following [49, 58], we focus on the time evolution of $(d/d_0)^{1.5}$, where d_0 is the initial droplet diameter, which is expected to be an almost linear function of time.

The experiments were performed for the following initial mass fractions of SiO_2 nanoparticles: 0%, 2% and 7%. As mentioned earlier, the ambient gas temperature was $T_g = 28.4$°C, relative humidity was 4.3%, and air velocity $U = 0.2$ m/s. The droplets were supported by two threads, both 0.105 mm in diameter. The initial droplet diameters were 2.20 mm (pure water), 2.19 mm (water with 2% nanoparticles), and 2.24 mm (water with 7% nanoparticles). The experiments with pure water were repeated twice, while the experiments with nanofluids were repeated three times for each initial concentration of SiO_2 nanoparticles. The results of the experiments were very close; they differed slightly, due to small differences (up to 4%) in the initial droplet radii. The results of only one experiment from each series of the experiments will be presented in this section.

Note that for this value of velocity, initial droplet diameter 2.2 mm, and air kinematic viscosity 15.89×10^{-6} m^2/s (at temperature 300 K) we obtain Re= 27.7. For thermal diffusivity of air equal to 22.5×10^{-6} m^2/s and mass diffusivity of water vapour in air 26×10^{-6} m^2/s (both at room temperature) [57] we obtain the following values of the Prandle and Schmidt numbers: Pr=0.7 and Sc=0.6. Using the simplest formulae for the estimation of the Nusselt and Sherwood numbers, assuming that both Spalding heat and mass transfer numbers are small [46]:

$$\mathrm{Nu} = 2 + 0.6\ \mathrm{Re}^{1/2}\mathrm{Pr}^{1/3},$$

$$\mathrm{Sh} = 2 + 0.6\ \mathrm{Re}^{1/2}\mathrm{Sc}^{1/3},$$

we obtain Nu$\approx$ 4.8 and Sc$\approx$ 4.7. Both these numbers are expected to decrease with time due to decreasing droplet diameters during the evaporation process. For finite Spalding heat and mass transfer numbers these values are expected to be slightly smaller. Note that a relatively large value of Re used in our experiments justifies the 1.5 power law for the time evolution of droplet diameters except at the initial stage of droplet evaporation (see [49] for the details).

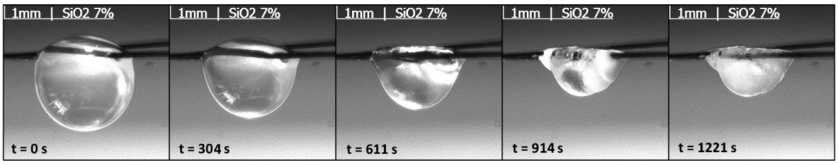

Fig. 3 Images of evaporating droplets with an initial mass fraction of SiO_2 7%.

The value of ambient air velocity in the experiments was selected to ensure that we had control over the influence of ambient air humidity on the evaporation process. Investigation of the effect of the ambient air velocity on droplet evaporation was beyond the scope of this paper.

Images of evaporating droplets with initial mass fraction of SiO_2 7% in the time range 0 – 1228 s are shown in Figure 3. At times close to $t = 921$ s the surface mass fraction of nanoparticles reached about 0.4, droplet size stopped reducing and a porous cenosphere-like structure was formed. As follows from this figure, the droplet shape is reasonably close to spherical until about $t = 600$ s (10 minutes), but at the later stage of its evaporation the deviations of the droplet shape from spherical are clearly seen. At this point the model used in our analysis becomes less reliable.

The normalised droplet diameters $(d/d_0)^{1.5}$ versus time (t) are shown in Figure 4. Calculations were performed until the mass fractions of nanoparticles at the droplet surface reached 0.4 when the formation of the cenosphere-like structure at the surface of the droplet was observed. As expected, both experimentally observed and predicted $(d/d_0)^{1.5}$ are almost linear functions of time except at the very initial stage (heat-up period) and the final stage of evaporation of droplets for an initial mass fraction of nanoparticles of 7% (we refer to [49] for a detailed discussion of the linear behaviour of this curve).

As can be seen in Figure 4, the agreements between observed and predicted values of droplet diameters are close before the cenosphere-like structure at the surface of the droplet is formed. This happened when the surface mass fraction of nanoparticles reached about 0.4 (calculations stopped). The deviation between the modelling and experimental results can be attributed to a number of factors which were not taken into account in the model, the most important of which is our assumption about the sphericity of the droplet (see [59] for the details). Once the cenosphere-like structure at the surface of the droplet begins to form, the model can no longer be used. Also, it can be seen in Figure 4 that there is almost no dependence of the evaporation rate of a droplet on the initial mass fraction of nanoparticles, observed experimentally and predicted by the model, until about $t = 300$ s. At later times, a slight increase in the evaporation rate with a decreasing initial mass fraction of nanoparticles is observed and predicted by the model. As mentioned earlier, at these times the predictions of the model become less reliable as the model does not consider the effect of non-sphericity of droplets.

The plots of the observed and predicted values of $T_g - T_s$ versus time for the same parameters as in Figure 4 are shown in Figure 5. The symbols show

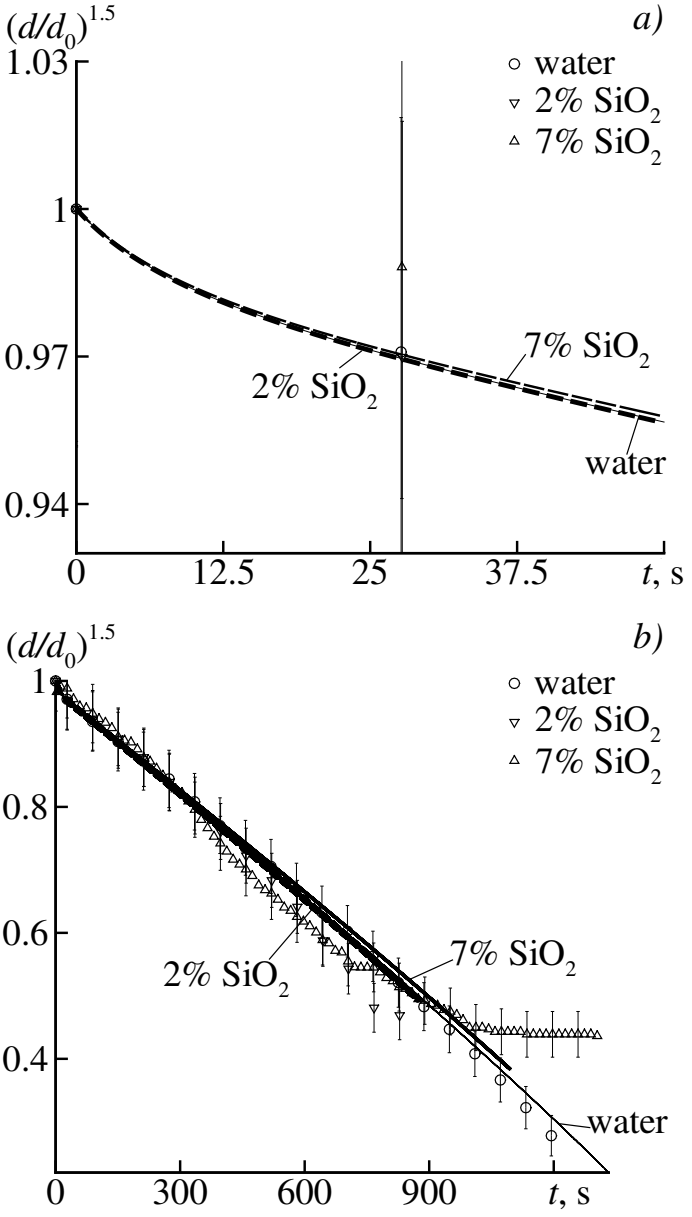

Fig. 4 Plots of $(d/d_0)^{1.5}$ versus time for water and nanofluids. Symbols refer to experimental data, circles – water, down (up) triangles – 2% (7%) SiO_2 nanofluid. Curves refer to the predictions of the model. Solid – water, dashed thick (thin) curve – 2% (7%) SiO_2 nanofluid, a) the initial 50 seconds (note big error bars), b) the entire period of observation.

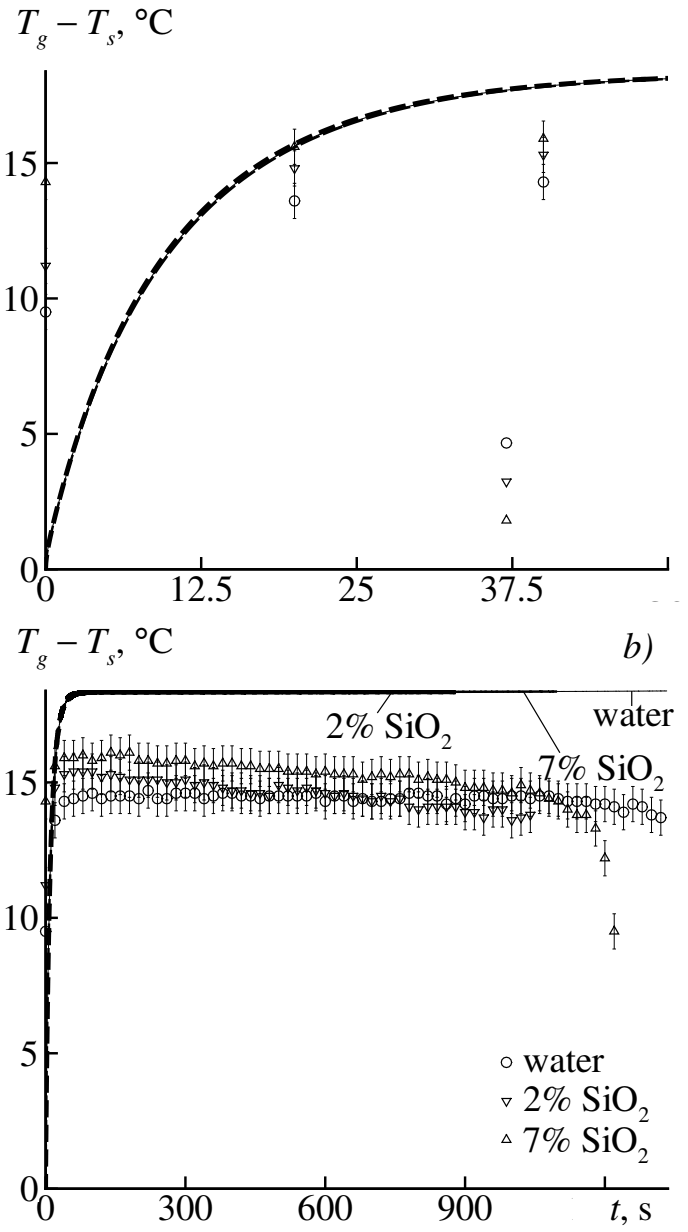

Fig. 5 Plots of $T_g - T_s$ versus time for water and the nanofluid. Symbols refer to experimental data, circles – water, down (up) triangles – 2% (7%) SiO_2 nanofluid. Curves show the predictions of the model. Solid – water, dashed thick (thin) curve – 2% (7%) SiO_2 nanofluid, a) the initial 50 seconds, b) the entire period of observation.

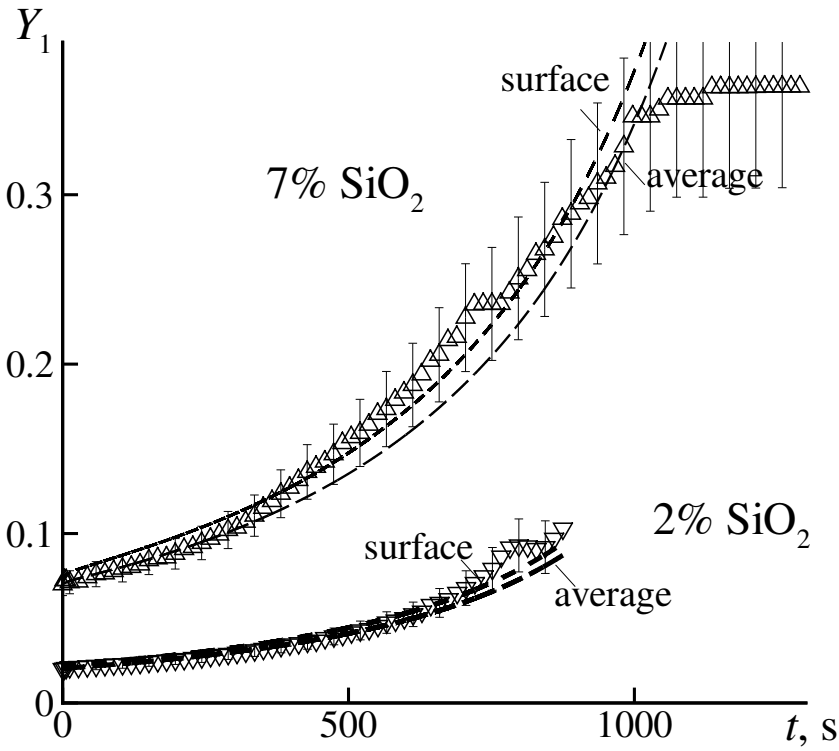

Fig. 6 Plots of average (lower curves) and surface (upper curves) mass fraction of SiO_2 (Y_1) versus time for the nanofluid. Symbols refer to experimental data, down (up) triangles – 2% (7%) SiO_2 nanofluid. Curves refer to the predictions of the model for the same values of input parameters as in Figures 4 and 5. Dashed thick (thin) curves refer to 2% (7%) SiO_2 nanofluids.

the experimental data. The observed difference $T_g - T_s$ initially increases and then slowly decreases with time. This result is compatible with those shown in Figure 2. Note that the modelling results presented are for the time up until the surface mass fraction of nanoparticles reached the threshold value of 0.4 when the porous structure at the droplet surface is expected to develop (see Section 3.1 for the details).

As follows from Figure 5, the predicted and observed initial increase in $T_g - T_s$ are very close. The observed maximal values of $T_g - T_s$ are slightly (several K) lower than the predicted ones. After about $t = 100$ s the predicted values of $T_g - T_s$ remain almost constant while the experimentally observed values of this parameter decrease with time. This might be related to a decrease in the temperature of ambient air in the vicinity of droplets with time, which is not taken into account in the model (T_g in the model is assumed to be constant).

Note that in the experiments, the results of which have been described, the droplet temperature reduces compared with its initial temperature which

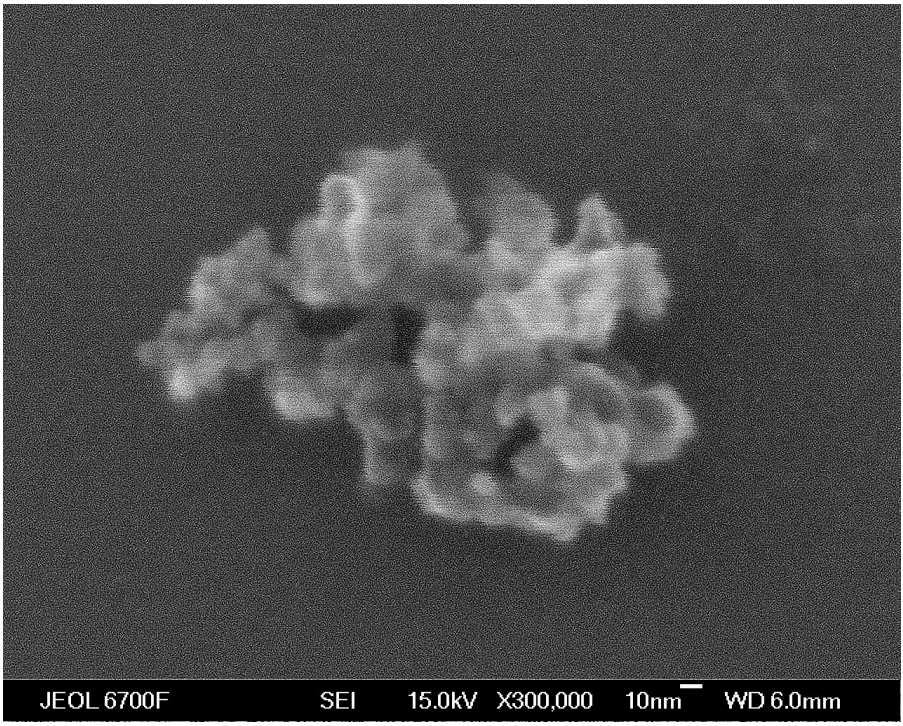

Fig. 7 Scanning electron microscope (SEM) image of an SiO_2 nanoparticle.

leads to droplet contraction. Unfortunately, we cannot separate the effects of droplet evaporation and the above-mentioned contraction (both of which are described by the model) based on our experimental data.

Plots of predicted average and surface mass fractions of SiO_2 and observed average mass fractions of SiO_2 (Y_1) versus time for the nanofluids with initial mass fractions of 2% and 7% of SiO_2 are presented in Figure 6. As follows from this figure, the predicted values of average and surface mass fractions of SiO_2 are rather close which indicates that the diffusion of nanoparticles in droplets is quick enough to maintain almost homogeneous distribution of these nanoparticles at all time instants. The agreement between the observed and predicted average values of Y_1 looks almost ideal until the cenosphere-like structure begins to form (when the initial mass fraction of nanoparticles is equal to 0.07) or the observations stopped (when the initial mass fraction of nanoparticles is equal to 0.02). This supports the applicability of our modelling approach to the investigation of the experimental data presented in the paper.

In the case of 7% of SiO_2 the value of $Y_1 = 0.4$ was reached after about 1030 s. This is consistent with the results shown in Figures 2, 3 and 4.

Note that the limiting mass fraction of nanoparticles of about 0.4 (when the porous structure at the droplet surface developed) is less than the maximal mass fraction of spherical particles corresponding to their maximal volume fraction of 0.61 predicted in [50] (see our discussion in Section 3.1). This is

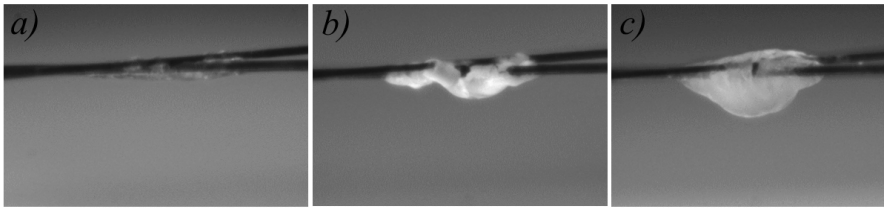

Fig. 8 Images of the residues of nanoparticles after the completion of the drying process: 'a', 'b' and 'c' refer to the cases in which the initial mass fractions of nanoparticles were 0.01, 0.02 and 0.07, respectively.

related to the non-sphericity and complex shapes of the nanoparticles used in our experiments. A typical SEM image of an SiO_2 nanoparticle is shown in Figure 7. Note that in other experiments this limiting mass fraction of nanoparticles at the droplet surface can be different from 0.4, but in all cases it was in the range 0.4-0.6.

Similar limiting mass fractions of nanoparticles can be expected for droplets of nanofluid with lower initial mass fractions of nanoparticles including those with mass fractions 1% and 2%. The relevant images of the residues of droplets after the completion of the drying process (including the image for the initial mass fraction 7%) are shown in Figure 8. As can be seen in this figure, although these residues are easily recognisable, the limiting mass fractions of nanoparticles cannot be easily measured for the cases of initial mass fractions 1% and 2% due to the complexity of the shapes of these residues.

5 Conclusions

The results of experimental studies and modelling of the evaporation of suspended water droplets containing silicon dioxide SiO_2 nanoparticles at initial mass fractions 0.02 and 0.07 are presented for the first time, to the best of the authors' knowledge. The initial droplet temperatures were the same as ambient temperatures (about 25°C). The experiments were performed at atmospheric pressure in the presence of air moving at a velocity of 0.2 m/s. The droplets were fixed on a crosshair of threads with diameters 105 μm. The time evolution of droplet diameters was measured with a Baumer vcxg-04m high-speed video. The surface temperatures were measured in the layer of thickness of not more than 9 μm with an NEC TH7102IR thermal imaging camera at wavelengths in the range 8 to 14 μm.

The experimental results were interpreted in terms of the previously developed model for multicomponent droplet heating and evaporation. In this model, droplets are assumed to be spherical and the analytical solutions to the heat transfer and species diffusion equations were incorporated into the numerical code and used at each time step of the calculations. Silicon dioxide nanoparticles were considered to be a non-evaporating component. The effect

of supporting threads was taken into account assuming that the heat supplied through them would be instantaneously and homogeneously distributed throughout the whole droplet volume.

It was demonstrated that both observed and predicted values of droplet diameters to the power 1.5 decrease almost linearly with time almost throughout droplet evaporation, and are only weakly affected by the presence of nanoparticles. This law was not followed at the very initial stage (the heat-up period) of droplet evaporation and in the final stages when the mass fraction of nanoparticles at the droplet surface reached about 0.4 and a cenosphere-like structure was formed. In this case, the effect of nanoparticles becomes dominant. The limiting average mass fraction of nanoparticles of about 0.4 is less than the maximal mass fraction of spherical particles corresponding to their maximal volume fraction of 0.61. This is related to the non-sphericity and complex shapes of the nanoparticles used in our experiments. The formation of this structure was not considered by the model used in the analysis.

Both predicted and observed droplet surface temperatures rapidly decreased during the initial stage of droplet evaporation. After about $t = 100$ s the predicted $T_g - T_s$ remained almost constant while the experimentally observed values of this parameter slowly decreased with time. This might be related to a slight decrease in the temperature of ambient air in the vicinity of droplets which was not considered in the model.

Both observed and predicted values of the average mass fraction of silicon dioxide were shown to increase with time until this mass fraction reached a value close to 0.4.

Acknowledgements

Work on this paper was supported by the Ministry of Science and Higher Education of the Russian Federation (grant no. 075-15-2021-575) (experimental studies of droplet evaporation processes by E.M. Starinskaya, N.B. Miskiv, A.D. Nazarov, V.V. Terekhov, and V.I. Terekhov), the Royal Society (UK) (Grant no. IEC 192007) (development and implementation of the mathematical model by O. Rybdylova and S.S. Sazhin), and the UKRI (Grant no. MR/T043326/1) (development and implementation of the mathematical model by O. Rybdylova).

References

[1] S.K. Das, S.U.S. Choi, W.Yu, T. Pradeep, Nanofluids: Science and Technology, John Wiley & Sons, Inc., Hoboken, New Jersey, 2008

[2] V.Y. Rudyak, A.V. Minakov, Modern Problems of Micro- and Nanofluidics, 'Nauka', Novosibirsk, 2016 (in Russian).

[3] M.J. Assael, K.D. Antoniadis, W.A. Wakeham, X. Zhang, Potential applications of nanofluids for heat transfer, Int. J. Heat and Mass Transfer 138

(2019) 597-607. doi.org/10.1016/j.ijheatmass transfer.2019.04.086

[4] G. Liang, I. Mudawar, Review of single-phase and two-phase nanofluid heat transfer in macro-channels and micro-channels, Int. J. Heat and Mass Transfer 136 (2019) 324-354. doi.org/10.1016/ j.ijheatmasstransfer.2019.02.086

[5] V.I. Terekhov, S.V., Kalinina, V.V. Lemanov, The mechanism of heat transfer in nanofluids: state of the art (review). Part 1. Synthesis and properties of nanofluids, Thermophys. Aeromech. 17 (2010) 1-14. doi.org/10.1134/S0869864310010014

[6] P. Katre, S. Balusamy, S. Banerjee, L.D. Chandrala, K.C. Sahu, Evaporation dynamics of a sessile droplet of binary mixture laden with nanoparticles, Langmuir 37 (2021) 6311-6321. doi.org/10.1021/acs.langmuir.1c00806

[7] L. Cheng, G. Xia, Q. Li & J.R. Thome, Fundamental issues, technology development, and challenges of boiling heat transfer, critical heat flux, and two-phase flow phenomena with nanofluids, Heat Transfer Eng. 40(16) (2019) 1301-1336, doi:.org/10.1080/01457632.2018.1470285

[8] S.J. Kim, T. McKrell, J. Buongiorno, L-W. Hu, Experimental study of flow critical heat flux in alumina-water, Zinc-Oxide- Water, and Diamond-Water nanofluids, J Heat Transf. 131 (2009) 043204-1. doi.org/10.1115/1.3072924

[9] Pin Chen. Enhancement of drops evaporation using nanoparticles and alcohols. Mechanics [physics.med-ph]. Université de Valenciennes et du Hainaut-Cambresis, 2018.

[10] X. Zhong, A. Crivoi, F. Duan, Sessile nanofluid droplet drying, Adv. Colloid and Interface Science 217 (2015) 13-30. doi.org/10.1016/j.cis.2014.12.003

[11] K. Sefiane, R. Bennacer, Nanofluids droplets evaporation kinetics and wetting dynamics on rough heated substrates, Adv. Colloid and Interface Sci. 147-148 (2009) 263-271. doi.org/10.1016/ j.cis.2008.09.011

[12] W.A. Sirignano, Fluid Dynamics and Transport of Droplets and Sprays, Cambridge Univ. Press, Cambridge, UK, 1999.

[13] R.-H. Chen, T.X. Phuoc, D. Martello, Effects of nanoparticles on nanofluid droplet evaporation, Int. J. Heat Mass Transf. 53, (2010) 3677-3682, doi.org/10.1016/j.ijheatmass transfer.2010.04.006

[14] R.-H. Chen, T.X. Phuoc, D. Martello, Surface tension of evaporating nanofluid droplets, Int. J. Heat Mass Transf., 54 (2011) 2459-2466. doi.org/10.1016/j.ijheatmasstransfer.2011.02.016

[15] W. Zhang, R. Shen, K. Lu, A. Ji, and Z. Cao, Nanoparticle enhanced evaporation of liquids: A case study of silicone oil and water, AIP Advances 2 (2012) 042119, doi.org/10.1063/1.4764294

[16] A.A. Bochkarev, V.I. Polyakova, Numerical modeling of acceleration of liquid evaporation by adding nanoparticles. Proc. Conference 'Modern problems of the dynamics of rarefied gases', Kutateladze Institute of Thermophysics SB RAS, July 26-29, 2013, Novosibirsk, pp. 66-68 (In Russian).

[17] V.A. Kumar, S.P. Sathian, Evaporation of a liquid droplet in the presence of a nanoparticle, J. of Heat Transf. 140 2018 054501, doi.org/10.1115/1.4038477.

[18] Y. Wei, W. Deng, R-H. Chen, Effects of insoluble nano-particles on nanofluid droplet evaporation, Int. J. Heat Mass Transf. 97 (2016) 725-734, doi.org/10.1016/j.ijheatmass transfer.2016.02.052.

[19] C.S. Handscomb, M. Kraft, A.E. Bayly, A new model for the drying of droplets containing suspended solids, Chemical Engin. Sci. 64 (2009) 628-637, doi.org/10.1016/j.ces.2008.04.051.

[20] A.V. Minakov, A.S. Lobasov, M.I. Pryazhnikov, L.S. Tarasova, N.Ya. Vasilenko V.Ya. Rudyak, Experimental study of the influence of nanoparticles on evaporation of fluids, Tech. Phys. 65(1) (2020) 29-36. doi.org/10.1134/S1063784220010181.

[21] V.I. Terekhov, N.E. Shishkin, Evaporation of water droplets containing carbon nanotubes, Tech. Phys. Lett. 38 (1) (2012) 25-28, doi.org/10.1134/S1063785012010142

[22] M. Moghiman, B. Aslani, Influence of nanoparticles on reducing and enhancing evaporation mass transfer and its efficiency, Int. J. of Heat and Mass Transf. 61 (2013) 114-118, doi.org/10.1016/j.ijheatmasstransfer.2013.01.057

[23] Y. Gan, L. Qiao, Evaporation characteristics of fuel droplets with the addition of nanoparticles under natural and forced convections, Int. J. of Heat and Mass Transf. 54 (2011) 4913-4922, doi.org/10.1016/j.ijheatmasstransfer.2011.07.003

[24] I. Javed, S.W. Baek, K. Waheed, G. Ali, S.O. Cho, Evaporation characteristics of kerosene droplets with dilute concentrations of ligand-protected aluminum nanoparticles at elevated temperatures, Combustion and Flame, 160 (2013) 2955-2963, doi.org/10.1016/j.combustflame.2013.07.007

[25] W.J. Gerken, A.V. Thomas, N. Koratkar, M.A. Oehlschlaeger, Nanofluid pendant droplet evaporation: Experiments and modeling. Int. J. of Heat and Mass Transf. 74 (2014) 263-268, doi.org/10.1016/j.ijheatmasstransfer.2014.03.031

[26] X. Wang, M. Dai, J. Wang, Y. Xie, G. Ren, Genzhu Jiang, Effect of ceria concentration on the evaporation characteristics of diesel fuel droplets, Fuel 236 (2019) 1577-1585, doi.org/10.1016/j.fuel.2018.09.085

[27] M. Dai, J. Wang, N. Wei, X. Wang, C. Xu, Experimental study on evaporation characteristics of diesel/cerium oxide nanofluid fuel droplets, Fuel 254 (2019) 115633, doi.org/10. 1016/j.fuel.2019.115633

[28] S. Tanvir, S. Biswas, L. Qiao, Evaporation characteristics of ethanol droplets containing graphite nanoparticles under infrared radiation, Int. J. of Heat and Mass Transfer 114 (2017) 541-549, doi.org/10.1016/j.ijheatmasstransfer.2017.06.059

[29] Y. Gan, L. Qiao, Radiation-enhanced evaporation of ethanol fuel containing suspended metal nanoparticles, Int. J. of Heat and Mass Transfer 55 (2012) 5777-5782, doi.org/10.1016/j. ijheatmasstransfer.2012.05.074

[30] Z. Said, M.H. Sajid, R. Saidur, M. Kamalisarvestani, N.A. Rahim, Radiative properties of nanofluids, Int. Comm. in Heat and Mass Transfer 46 (2013) 74-84, doi.org/10.1016/j.icheatmass transfer.2013.05.013

[31] D. Jing, D. Song, Optical properties of nanofluids considering particle size distribution: Experimental and theoretical investigations, Renewable and Sustainable Energy Rev. 78 (2017) 452-465, doi.org/10.1016/j.rser.2017.04.084

[32] S.P. Fisenko, Y.A. Khodyko, Brownian diffusion inside a micron-sized droplet and the morphology of ensembles of nanoparticles, J. Eng. Phys. Thermophys. 86 (2013) 349-355. https://doi.org/10.1007/s10891-013-0840-0.

[33] F.R. Siddiqui, C.Y. Tso, S.C. Fu, H.H. Qiu, C.Y.H. Chao, Evaporation and wetting behavior of silver-graphene hybrid nanofluid droplet on its porous residue surface for various mixing ratios, Int. J. Heat Mass Transf. 153 (2020). https://doi.org/10.1016/j.ijheatmasstransfer.2020.119618.

[34] H.C. Chan, S. Paik, J.B. Tipton, K.D. Kihm, Effect of nanoparticle sizes and number densities on the evaporation and dryout characteristics for strongly pinned nanofluid droplets, Langmuir. 23 (2007) 2953-2960. https://doi.org/10.1021/la061661y.

[35] E. Starinskaya, A.D. Nazarov, N. Miskiv, S. Starinskiy, Effect of SiO_2 nanoparticle addition on the evaporation of a suspended water droplet, Heat Transf. Res. 53 (2022) 43-56. https://doi.org/10.1615/heattransres.2022041024.

[36] R. Mulka, A. Kujawska, B. Zajaczkowski, S. Mancin, M.H. Buschmann, Drying silica-nanofluid droplets, colloids and surfaces A: Physicochemical and Engineering Aspects, 623 (2021) 126730. doi.org/10.1016/j.colsurfa.2021.126730

[37] N.B. Vagraftik, Handbook of Thermophysical Properties of Fluids, Nauka Publishing House, Moscow, 1972 (in Russian).

[38] K. Han, G. Song, X. Ma, B. Yang, An experimental and theoretical study of the effect of suspended thermocouple on the single droplet evaporation, Appl. Therm. Eng. 101 (2016) 568-575, doi.org/10.1016/j.applthermaleng.2015.12.022.

[39] J.R. Yang, S.C. Wong, An experimental and theoretical study of the effects of heat conduction through the support fiber on the evaporation of a droplet in a weakly convective flow, Int. J. Heat Mass Transf. 45 (2002) 4589-4598. doi.org/10.1016/S0017-9310(02)00164-3.

[40] D. Brutin, Influence of relative humidity and nano-particle concentration on pattern formation and evaporation rate of pinned drying drops of nanofluids, Colloids Surfaces A Physicochem. Eng. Asp. 429 (2013) 112-120. doi.org/10.1016/j.colsurfa.2013.03.012.

[41] P. Tartarini, M.A. Corticelli, L. Tarozzi, Dropwise cooling: Experimental tests by infrared thermography and numerical simulations, Appl. Therm. Eng. 29 (2009) 1391-1397. doi.org/10.1016/j.applthermaleng.2008.06.011.

[42] A.A. Fedorets, L.A. Dombrovsky, A.M. Smirnov, The use of infrared self-emission measurements to retrieve surface temperature of levitating water droplets, Infrared Phys. Technol. 69 (2015) 238-243. doi.org/org/10.1016/j.infrared.2015.02.005.

[43] V.Y. Borodulin, V.N. Letushko, M.I. Nizovtsev, A.N. Sterlyagov, Determination of parameters of heat and mass transfer in evaporating drops, Int. J. Heat Mass Transf. 109 (2017) 609-618. doi.org/10.1016/j.ijheatmasstransfer.2017.02.042

[44] S.S. Sazhin, O. Rybdylova, A.S. Pannala, S. Somavarapu, S.K. Zaripov, A new model for a drying droplet, Int. J. Heat and Mass Transf. 122 (2018) 451-458. doi.org/10.1016/j.ijheatmasstransfer.2018.01.094

[45] P.A. Strizhak, R.S. Volkov, G. Castanet, F. Lemoine, O. Rybdylova, S.S. Sazhin, Heating and evaporation of suspended water droplets: Experimental studies and modelling, Int. J. Heat Mass Transf. 127 (2018) 92-106. doi.org/10.1016/j.ijheatmasstransfer.2018.06.103

[46] S.S. Sazhin, Droplets and Sprays: Simple Models of Complex Processes. Springer (series 'Mathematical Engineering') (2022). DOI 10.1007/978-1-4471-6386-2

[47] B. Abramzon, W.A. Sirignano, Droplet vaporization model for spray combustion calculations, Int. J Heat Mass Transf. 32 (1989) 1605-1618. doi.org/10.1016/0017-9310(89)90043-4

[48] D.V. Antonov, R.M. Fedorenko, P.A. Strizhak, Z. Nissar, S.S. Sazhin, Puffing/micro-explosion in composite fuel/water droplets heated in flames, Combustion and Flame 233 (2021) 111599. doi.org/10.1016/j.combustflame.2021.111599

[49] E.M. Starinskaya, N.B. Miskiv, A.D. Nazarov, V.V. Terekhov, V.I. Terekhov, O.D. Rybdylova, S.S. Sazhin, Evaporation of water/ethanol droplets in an air flow: experimental study and modelling, Int. J. Heat Mass Transf, 177 (2021) 121502. doi.org/10.1016/j.ijheatmass transfer.2021.121502

[50] B.S Radovskii, Random packing density of spherical solids, Reports of the Academy of Sciences of the USSR: Mechanics of a Rigid Body Issue 4 (1972) 184-190.

[51] A. Einstein, Eine neue Bestimmung der Moleküldimensionen, Ann. Phys. 324 (2) (1906) 289-306

[52] S.S. Sazhin, M. Al Qubeissi, R. Nasiri, V.M. Gun'ko, A.E. Elwardany, F. Lemoine, F. Grisch, M.R. Heikal, A multi-dimensional quasi-discrete model for the analysis of Diesel fuel droplet heating and evaporation. Fuel 129 (2014) 238-266. doi.org/10.1016/j.fuel.2014.03.028

[53] R.B. Bird, E.W. Stewart, E.N. Lightfoot, Transport Phenomena. Second Edition. New York, Chichester: Wiley & Sons, 2002.

[54] C.M. Silva, H. Li, E.A. Macedo, Models for self-diffusion coefficients of dense fluids, including hydrogen-bonding substances. Chemical Engineering Science 53 (1998) 2423-2429. doi.org/10.1016/S0009-2509(98)00037-2

[55] J.C. Maxwell, A Treatise on Electricity and Magnetism, third ed., Oxford University Press, London, 1892.

[56] C.L. Yaws, editor, Thermophysical Properties of Chemicals and Hydrocarbons. William Andrew Inc., 2008.

[57] B.E. Poling, J.M. Prausnitz, J.P. O'Connell, The Properties of Gases and Liquids, Fifth Edition, 2001. doi.org/10.1002/aic.690240634

[58] V.I. Terekhov, V.V. Terekhov, N.E. Shishkin, K.Ch. Bi, Heat and mass transfer in disperse and porous media: investigation of non-stationary evaporation of liquid droplets, J. of Engineering Physics and Thermophysics 83(5) (2010) 883-890. doi.org/10.1007/s10891-010-0410-7

[59] V.S. Zubkov, G.E. Cossali, S. Tonini, O. Rybdylova, C. Crua, M. Heikal, S.S. Sazhin, Mathematical modelling of heating and evaporation of a spheroidal droplet, Int. J. Heat Mass Transf. 108-A (2017) 2181-2190. doi.org/10.1016/j.ijheatmasstransfer.2016.12.074